RSC Advances

ROYAL SOCIETY OF CHEMISTRY

www.rsc.org/advances

RSC. Adv

ARTICLE

A novel single-phase white light emitting phosphor $Ca_9La(PO_4)_5(SiO_4)F_2:Dy^{3+}$: synthesis, crystal structure and luminescence property

Received 00th January 20xx,
Accepted 00th January 20xx

DOI: 10.1039/x0xx00000x

www.rsc.org/

Haikun Liu[a], Libing Liao[a,*], Maxim S. Molokeev[b,c], Qingfeng Guo[a], Yuanyuan Zhang[a], Lefu Mei[a,*]

A novel single-phase white light emitting phosphor $Ca_9La(PO_4)_5(SiO_4)F_2:Dy^{3+}$ was prepared through a traditional high temperature solid state technology. The crystal structures of $Ca_9La(PO_4)_5(SiO_4)F_2$ with or without Dy^{3+} ions were refined by the Rietveld method. The diffuse reflection spectra, excitation spectra, emission spectra, and decay times were characterized to investigate the photoluminescence properties for application in white light-emitting diodes. The results showed that $Ca_9La(PO_4)_5(SiO_4)F_2:Dy^{3+}$ phosphor could effciently assimilate the *n*-UV light and emit blue (~485 nm) and yellow light (~580 nm), originating from the *f-f* transitions of Dy^{3+}. The critical Dy^{3+} quenching concentration (QC) was determined to be about 15 mol%, and the corresponding QC mechanism was verified to be the dipole–dipole interaction. Additional, the emission colors of all samples located close to the ideal white light region, and the optimal chromaticity coordinates and correlated color temperature (CCT) were determined to be (x = 0.338, y = 0.336) and 5262 K. All the above results indicated that the as-prepared $Ca_9La(PO_4)_5(SiO_4)F_2:Dy^{3+}$ phosphor could be served as a promising candidate for white-light *n*-UV-LEDs.

1 Introduction

Over the past few decades, white-light-emitting diodes (*w*-LEDs) are considered as the most potential lighting source after incandescent lamp and energy saving lamp, which have fascinated considerable attention because of their favorable advantages of high luminous efficiency, reliability and environmentally friendly characteristics [1-3]. Presently, the most prevalent *w*-LEDs in the market generally can be fabricated by a combination of a blue InGaN chip and the yellow-emitting YAG:Ce phosphor on basis of the phosphor-converted emission mechanism. However, this approach faces a low color rendering index and a high correlated color temperature due to the lack of sufficient red component [4, 5]. Accordingly, another alternative method on fabricating *w*-LEDs is generated by means of near-ultraviolet (*n*-UV) chip LED assigned with the mixture of tricolor (blue, green and red) phosphors. This method also faces some disadvantages such as low luminescent efficiency due to the reabsorption of the blue light by the red and green phosphors [6]. Therefore, it is instant for the development of a single-phase white-light emitting phosphor to widespread use in *w*-LEDs application.

As an important member in solid state phosphor family, the apatite structure compounds have been extensively studied in solid-state illumination and display manufacturing owing to their stable and adjustable structure for optical materials [7, 8]. It is well known that the typical apatite compound has an iso-structure to the nature mineral fluorapatite $Ca_{10}(PO_4)_6F_2$, which belongs to the hexagonal symmetry system (space group of $P6_3/m$) with a general chemical formula as $A_{10}(PO_4)_6Z_2$, where A often represents divalent cations such as Ca^{2+}, Mg^{2+}, Ba^{2+}, Fe^{2+}, Sr^{2+}, Mn^{2+}, Pb^{2+} and so on. Meanwhile, $[PO_4]^{3-}$ can also be isomorphically substituted by $[SiO_4]^{4-}$, $[BO_4]^{5-}$, and $[VO_4]^{3-}$ anion groups under different conditions. And Z is always denoted by F, Cl, Br, or O [9-12]. Since apatite-type compound possesses the capability of being substituted by versatile ions and forming host structure changeable solid solution, which may endow tunable luminescence and outstanding luminescent properties. That is to say, it is very interesting to build up new inorganic framework to obtain new compounds with apatite structure. Hitherto, several single-component white light emitting phosphors with apatite-type structure suitable for *n*-UV-pumped *w*-LED have been reported, such as, $Ca_2La_8(GeO_4)_6O_2:Eu^{3+}/Dy^{3+}$ [13], $Mg_2Y_8(SiO_4)_6O_2:Ce^{3+}/Tb^{3+}/Sm^{3+}$ [14] and $Sr_{3.5}Y_{6.5}O_2(PO_4)_{1.5}(SiO_4)_{4.5}:Ce^{3+}/Tb^{3+}/Mn^{2+}$ [15]. Recently, as a member of trivalent rare earth ions, dysprosium (Dy^{3+}) ions have been received intensively research interests and widely used in luminescence materials because of their unique luminescence properties [16-18]. Customarily, Dy^{3+} ions generate two dominant emissions in blue (475-500 nm) and yellow (570-

[a] Beijing Key Laboratory of Materials Utilization of Nonmetallic Minerals and Solid Wastes, National Laboratory of Mineral Materials, School of Materials Science and Technology, China University of Geosciences, Beijing, 100083, China.
[b] Laboratory of Crystal Physics, Institute of Physics, SB RAS, Krasnoyarsk 660036, Russia
[c] Department of Physics, Far Eastern State Transport University, Khabarovsk 680021, Russia
* Corresponding authors: E-mail address: clayl@cugb.edu.cn and mlf@cugb.edu.cn

600 nm) regions, which correspond to $^4F_{9/2} \rightarrow {}^6H_{15/2}$ (magnetic dipole transition) and $^4F_{9/2} \rightarrow {}^6H_{13/2}$ (electric dipole transition) transitions, respectively [19]. To our knowledge, the electric dipole transitions of Dy^{3+} ions can be easily affected by the crystal field environment of the host lattice rather than the magnetic dipole transitions of Dy^{3+} ions. Thus, it is an effective strategy to obtain white light emission in Dy^{3+} activated luminescent materials by adjusting the chemical environment of the matrix. Consequently, we demonstrated a novel single-component white-light phosphor $Ca_9La(PO_4)_5(SiO_4)F_2:Dy^{3+}$ with apatite structure for UV-light emitting diodes via a high-temperature solid-state technology. In addition, the concentration quenching as well as lifetime studies of Dy^{3+} in $Ca_9La(PO_4)_5(SiO_4)F_2$ phosphor was carried out in detail.

2 Experimental

Traditional high-temperature solid-state reaction method was employed to prepare $Ca_9La_{1-x}(PO_4)_5(SiO_4)F_2:xDy^{3+}$ phosphors. $CaCO_3$, $(NH_4)_2HPO_4$, SiO_2, NH_4HF_2, and Dy_2O_3 were mixed and ground according to the given stoichiometric ratio. An additional amount of NH_4HF_2 was mixed as flux and balanced the loss of F source at high temperature. Stoichiometric amounts of reactants were thoroughly mixed by grinded together in an agate mortar with a small amount of ethanol, then the final mixture was placed into an alumina crucible and annealed at 1450°C in a reducing atmosphere (5% H_2 + 95% N_2) for 5 h. After this, the samples were furnace-cooled to room temperature, and ground again into powder for measurement.

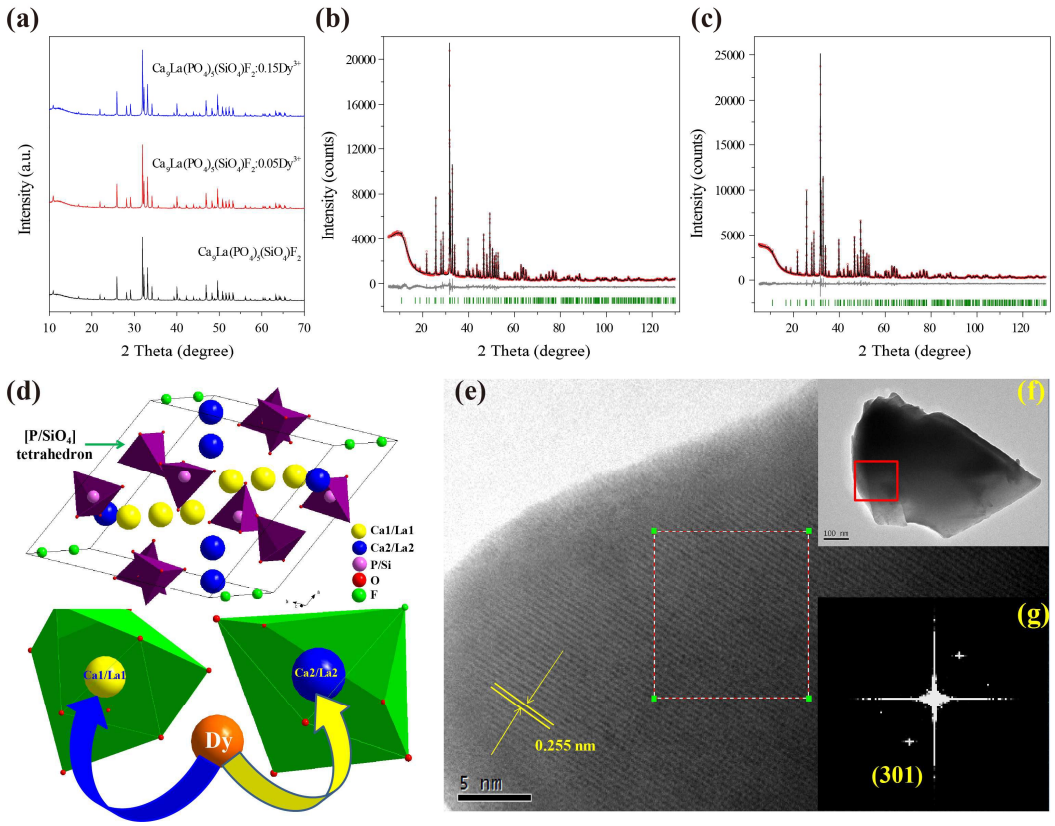

Fig. 1 (a) XRD patterns of as-prepared $Ca_9La(PO_4)_5(SiO_4)F_2$, $Ca_9La_{0.95}(PO_4)_5(SiO_4)F_2:0.05Dy^{3+}$ and $Ca_9La_{0.85}(PO_4)_5(SiO_4)F_2:0.15Dy^{3+}$ phosphors; Difference Rietveld plots of $Ca_9La(PO_4)_5(SiO_4)F_2$ **(b)** and $Ca_9La_{0.9}Dy_{0.1}(PO_4)_5(SiO_4)F_2$ **(c)**; **(d)** Crystal structure of $Ca_9La(PO_4)_5(SiO_4)F_2$, the coordination sphere and corresponding coordination polyhedron of Ca/La(I) ion and Ca/La(II) ion. **(e,f)** HRTEM images of $Ca_9La(PO_4)_5(SiO_4)F_2$ and the fast Fourier transforms (FFTs) of the relevant HRTEM images **(g)**.

X-ray diffraction (XRD) patterns were recorded using an X-ray powder diffractometer (XD-3, PGENERAL, China) with Cu-Kα radiation (λ = 0.15406 nm) operated at 40 kV and 30 mA. The continuous scanning rate (2θ ranging from 10° to 70°) used as phase determination was 8° (2θ)/min. The powder diffraction data of $Ca_9La(PO_4)_5(SiO_4)F_2$ and $Ca_9La_{0.9}Dy_{0.1}(PO_4)_5(SiO_4)F_2$ for Rietveld analysis were collected at room temperature with a Bruker D8 ADVANCE powder diffractometer (Cu-Kα radiation) and linear VANTEC detector. The step size of 2θ was 0.02°, and the counting time was 3s per step. Rietveld refinement was performed by using TOPAS 4.2 [20]. The measures of PL and photoluminescence excitation (PLE) spectra were carried out by a fluorescence spectrophotometer (F-4600, HITACHI, Japan) equipped with a photomultiplier tube operating at 400V, and a 150W Xe lamp was used as the excitation lamp. A 400 nm cutoff filter was used in the measurement to eliminate the second-order emission of source radiation. The diffuse-reflectance spectra

(DRS) were recorded by UV-Visible spectrometer (TU-1901, China) with integration sphere. The room-temperature luminescence decay curves were obtained from a spectrofluorometer (Horiba, Jobin Yvon TBXPS) using a tunable pulse laser radiation as the excitation. All measurements were carried out at room temperature.

3 Results and discussion

3.1 Crystal Structure of $Ca_9La(PO_4)_5(SiO_4)F_2$

Fig. 1a shows the XRD profiles of as-prepared $Ca_9La(PO_4)_5(SiO_4)F_2$, $Ca_9La_{0.95}(PO_4)_5(SiO_4)F_2$:0.05$Dy^{3+}$ and $Ca_9La_{0.85}(PO_4)_5(SiO_4)F_2$:0.15$Dy^{3+}$ phosphors. It is obvious that all the observed diffraction peaks are well indexed to the phases of $Ca_5(PO_4)_3F$ (JCPDS No. 15-0876) and no second phase is observed, which confirmed that the doping Dy^{3+} ions are completely incorporated into the host lattice and do not cause significant changes in the host.

In order to further check the crystal structure of the synthesized phosphor, the Rietveld structural refinements for $Ca_9La(PO_4)_5(SiO_4)F_2$ and $Ca_9La_{0.90}(PO_4)_5(SiO_4)F_2$:0.10$Dy^{3+}$ compounds were performed based on the TOPAS 4.2 program. Almost all peaks were indexed by hexagonal cell ($P6_3/m$) with parameters very close to $Ca_9La(PO_4)_5(SiO_4)F_2$ published earlier [21, 22]. Therefore this crystal structure was taken as starting model for Rietveld refinement. In this study, two independent sites of Ca were occupied by Ca, La and Dy ions with refined occupation and we assume the sum of occupancies in each site equals 1. Occupancies of P and Si in site were fixed according to suggested formula. No detectable impurity phase was observed in the obtained samples and we found all the observed peaks satisfy the reflection condition. The observed, calculated peaks and their difference for the Rietveld refinement are shown in Fig. 1b and Fig. 1c. Moreover, the final refined residual factors and refined structural parameters are summarized in Table 1, Table 2 and Table 3. It can be seen that all of the observed peaks satisfy the reflection condition and converge to R_{exp} = 3.33%, R_{wp} = 5.63%, R_p = 4.10 %, χ^2 = 1.69 in the refinement of the $Ca_9La(PO_4)_5(SiO_4)F_2$ compound and R_{exp} = 3.63%, R_{wp} = 5.55%, R_p = 4.03 %, χ^2 = 1.53 in the refinement of the $Ca_9La_{0.9}Dy_{0.1}(PO_4)_5(SiO_4)F_2$ compound, respectively. The unit cell parameters obtained for $Ca_9La(PO_4)_5(SiO_4)F_2$ are a = 9.432 Å, c = 6.926 Å, and V = 533.61 $Å^3$, which are larger than those for $Ca_9La_{0.9}Dy_{0.1}(PO_4)_5(SiO_4)F_2$ shown in Table 1. The larger cell parameters are ascribed to the larger-sized La atoms as compared with Dy atoms.

Table 1. Main parameters of processing and refinement of the samples.

Compound	$Ca_9La(PO_4)_5(SiO_4)F_2$	$Ca_9La_{0.9}Dy_{0.1}(PO_4)_5(SiO_4)F_2$
Sp.gr.	$P6_3/m$	$P6_3/m$
a, Å	9.4320(2)	9.4272(2)
c, Å	6.9261(1)	6.9216(1)
V, $Å^3$	533.61(2)	532.72(2)
Z	1	1
$Int_{2\theta}$, º	5-130	5-130
N_{re}	335	335
N_{rp}	51	51
R_{wp}, %	5.63	5.55
R_p, %	4.10	4.03
R_{exp}, %	3.33	3.63
χ^2	1.69	1.53
R_B, %	1.63	2.11

Table 2. Fractional atomic coordinates and isotropic displacement parameters of the $Ca_9La_{0.9}Dy_{0.1}(PO_4)_5(SiO_4)F_2$ compound.

	x	y	z	B_{iso}	Occ.
La1	2/3	1/3	-0.0003 (6)	1.3 (1)	0.042 (3)
Ca1	2/3	1/3	-0.0003 (6)	1.3 (1)	0.958 (3)
La2	0.2395 (2)	-0.0115 (3)	1/4	1.0 (1)	0.158 (5)
Ca2	0.2395 (2)	-0.0115 (3)	1/4	1.0 (1)	0.842 (5)
Si	0.3990 (4)	0.3698 (3)	1/4	0.6 (1)	1/6
P	0.3990 (4)	0.3698 (3)	1/4	0.6 (1)	5/6
O1	0.5892 (8)	0.4637 (9)	1/4	1.5 (1)	1
O2	0.3288 (7)	0.4849 (8)	1/4	1.5 (1)	1
O3	0.3379 (5)	0.2592 (5)	0.0689 (6)	1.5 (1)	1
F	0	0	1/4	1.5 (1)	1

Table 3. Fractional atomic coordinates and isotropic displacement parameters of the $Ca_9La(PO_4)_5(SiO_4)F_2$ compound.

	x	y	z	B_{iso}	Occ.
La1	2/3	1/3	-0.0013 (4)	1.24 (8)	0.033 (2)
Ca1	2/3	1/3	-0.0013 (4)	1.24 (8)	0.964 (2)
Dy1	2/3	1/3	-0.0013 (4)	1.24 (8)	0.0036 (2)
La2	0.2401 (2)	-0.0109 (2)	1/4	1.01 (8)	0.132 (3)
Ca2	0.2401 (2)	-0.0109 (2)	1/4	1.01 (8)	0.854 (3)
Dy2	0.2401 (2)	-0.0109 (2)	1/4	1.01 (8)	0.0147 (3)
Si	0.3984 (3)	0.3684 (3)	1/4	0.86 (9)	1/6
P	0.3984 (3)	0.3684 (3)	1/4	0.86 (9)	5/6
O1	0.5876 (6)	0.4650 (6)	1/4	1.4 (1)	1
O2	0.3270 (5)	0.4859 (5)	1/4	1.4 (1)	1
O3	0.3353 (4)	0.2529 (4)	0.0718 (4)	1.4 (1)	1

As mentioned previously, $Ca_9La(PO_4)_5(SiO_4)F_2$ belongs to apatite-type compound, which crystallizes in a hexagonal symmetrical system with space group $P6_3/m$ and the detailed crystal structure diagram of $Ca_9La(PO_4)_5(SiO_4)F_2$ compound is given in Fig. 1d. In this structure, there are two kinds of cationic sites labeled Ca/La(I) and Ca/La(II), the Ca/La(I) site is defined as being nine-fold coordinated with C_3 point symmetry, and Ca/La(II) is defined as being seven-fold coordinated with C_s point symmetry, respectively. As depicted in Fig. 1d, the Ca/La(I) site is surrounded by nine O atoms: three O(1), three O(2) and three O(3), forming a CaO_9-polyhedron with six short and three long Ca–O bonds. While the Ca/La(II) site is coordinated by six oxygen atoms (O(1), O(2), four O(3), and a fluorine atom forming an irregular CaO_6F-polyhedron [22]. Considering the effective ionic radii and charge balance of

cations with different coordination number (CN), the activators Dy^{3+} ions are predictable to occupy the La^{3+} sites randomly in the $Ca_9La(PO_4)_5(SiO_4)F_2$ host, because the effective ionic radii of Dy^{3+} (r = 0.97 Å for CN = 7 and r = 1.083 Å for CN = 9) is closest to that of La^{3+} (r = 1.10 Å for CN = 7 and r = 1.216 Å for CN = 9) [23]. The fine local structures of $Ca_9La(PO_4)_5(SiO_4)F_2$ are further examined by HRTEM, and the fast Fourier transform (FFT) images shown in Fig. 1e-g. It can be seen in Fig. 1e, the lattice fringes with a d spacing of 0.255 nm through the solved structure of the compound by refinement, which could be assigned to (301) plane. The $d_{(301)}$ enlarged ($d_{(301)}$ of 0.251 nm for $Ca_5(PO_4)_3F$ compound) slightly owing to the increase of the cell parameters with the substitution of La^{3+}/Si^{4+} for Ca^{2+}/P^{5+} ions as compared with the $Ca_5(PO_4)_3F$ compound.

3.2 Photoluminescence properties of $Ca_9La(PO_4)_5(SiO_4)F_2:Dy^{3+}$

The photoluminescence excitation (PLE) spectra and PL spectra of $Ca_9La_{0.85}(PO_4)_5(SiO_4)F_2$:0.15$Dy^{3+}$ under different monitoring wavelengths are demonstrated in Fig. 2a. Upon 352 and 387 nm excitation, this phosphor exhibits two similar prominent emission peaks in the visible wavelength region, one is locating in the blue region centered at 485 nm, which is attributed to the $^4F_{9/2}\rightarrow{}^6H_{15/2}$ (magnetic dipole transition) of the doped Dy^{3+} ions and the other is locating in the yellow region centered at 580 nm, which is corresponding to the $^4F_{9/2}\rightarrow{}^6H_{13/2}$ (electrical dipole transition) of the doped Dy^{3+} ions. Furthermore, few weak bands appeared in the red region, which is ascribed to $^4F_{9/2}\rightarrow{}^6H_{11/2}$ transition of the doped Dy^{3+} ions in $Ca_9La_{0.85}(PO_4)_5(SiO_4)F_2$:0.15$Dy^{3+}$ phosphors [24].

The PLE spectrum of $Ca_9La_{0.85}(PO_4)_5(SiO_4)F_2$:0.15$Dy^{3+}$ monitored at the blue region emission of Dy^{3+} (485 nm) is in consistent with that monitored at the yellow region emission of Dy^{3+} (580 nm) except for the tiny difference of the relative intensity. It is obvious that several sharp excitation peaks are found in the wavelength region of 275–500 nm to appear at 300, 326, 352, 363, 390, 428, 453 and 471 nm, which could be assigned to transitions from the $^6H_{15/2}$ ground state to the excited states of Dy^{3+} $^6F_{1/2}$, $^6P_{3/2}$, $^6P_{7/2}$, $^6P_{5/2}$, $^4I_{13/2}$, $^4G_{11/2}$, $^4I_{15/2}$, and $^4F_{9/2}$ levels, respectively. The proposed energy levels scheme of Dy^{3+} ions in $Ca_9La(PO_4)_5(SiO_4)F_2$ host upon excitation with UV radiation is presented in Fig. 2b. In view of the intense absorption band from 300-500 nm, the as-prepared $Ca_9La(PO_4)_5(SiO_4)F_2:Dy^{3+}$ phosphor can be used as a potential phosphor for UV/NUV LED lighting.

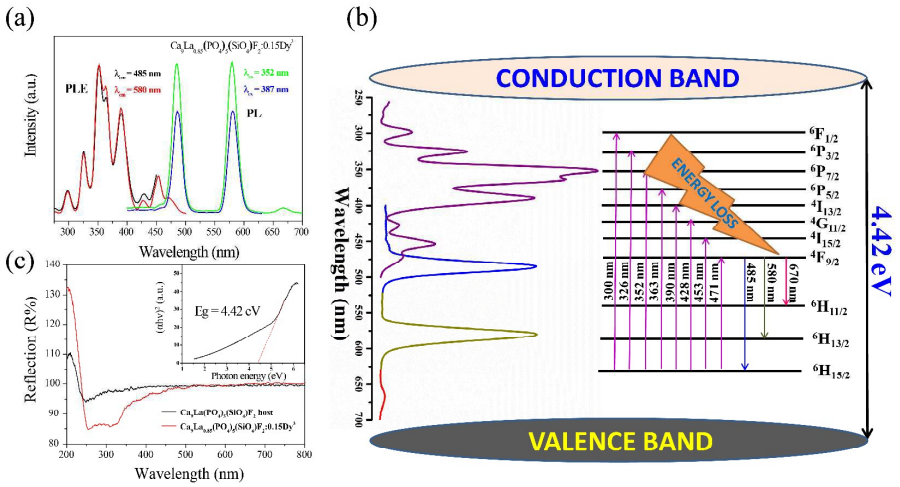

Fig. 2 (a) Excitation (λ_{em} = 485 and 580 nm) and emission (λ_{ex} = 352 and 387 nm) spectra of $Ca_9La_{0.85}(PO_4)_5(SiO_4)F_2$.:0.15$Dy^{3+}$. **(b)** PLE ($\lambda_{em}$ = 580 nm) and PL (λ_{ex} = 352 nm,) spectra with the energy level diagram of Dy^{3+} in the $Ca_9La(PO_4)_5(SiO_4)F_2$ phosphor at RT.**(c)** Diffuse reflection spectra of $Ca_9La(PO_4)_5(SiO_4)F_2$ host and $Ca_9La_{0.85}(PO_4)_5(SiO_4)F_2$:0.15$Dy^{3+}$ phosphor. Insert shows the absorption spectra of $Ca_9La(PO_4)_5(SiO_4)F_2$ matrix calculated by the Kubelka-Munk equation.

The UV-Vis reflection spectra of $Ca_9La(PO_4)_5(SiO_4)F_2$ host and $Ca_9La_{0.85}(PO_4)_5(SiO_4)F_2$:0.15$Dy^{3+}$ are described in Fig. 2c. The $Ca_9La(PO_4)_5(SiO_4)F_2$ matrix exhibits an energy absorption in the region with wavelength less than 300 nm and a high reflection ranging from 300 to 800 nm. The band gap of the virgin $Ca_9La(PO_4)_5(SiO_4)F_2$ can be estimated according to the following formula:[25, 26]

$$[F(R_\infty)h\nu]^n = A(h\nu - E_g) \qquad (1)$$

where $h\nu$ is the photon energy, A is a proportional constant, E_g is the value of the band gap, n = 2 for a direct transition or 1/2 for an indirect transition, and F(R∞) is Kubelka–Munk function which is defined as : [25, 26]

$$F(R_\infty) = (1-R)^2/2R = K/S \qquad (2)$$

where R, K and S are the reflection, the absorption and the scattering coefficient, respectively. As illustrated in the insert of Fig. 2c the band gap energy of the $Ca_9La(PO_4)_5(SiO_4)F_2$ host is estimated to be about 4.42 eV from the extrapolation of the line for $[F(R\infty)h\nu]^2$ = 0. With the activator Dy^{3+} introduced into the $Ca_9La(PO_4)_5(SiO_4)F_2$ host, a strong broad absorption band, attributing to the characteristic absorption of the Dy^{3+} ions

appeared in the 300-500 nm *n*-UV range, which matches well with its excitation spectra.

Fig. 3a gives PL spectra of $Ca_9La_{1-x}(PO_4)_5(SiO_4)F_2$:$xDy^{3+}$ (x = 0.01–0.50) under the excitation of 352 nm. According to the inset of Fig. 3a, the optimal doping concentration of Dy^{3+} in $Ca_9La_{1-x}(PO_4)_5(SiO_4)F_2$:$xDy^{3+}$ is fixed at x = 0.15, then the PL intensity begins to decrease, which could be ascribed to the internal concentration quenching effect via energy transfer from one activator to another. The interaction type between sensitizers or between sensitizer and activator can be estimated via the following equation:[27-29]

$$\frac{1}{x} = k[1+\beta(x)^{\theta/3}]^{-1} \qquad (3)$$

in which x is the concentration of activation, which is more than the critical concentration K and β are constants under the same excitation condition of host lattice, I/x is the emission intensity (I) per activator concentration (x) and ϑ is a function of electric multipolar character. ϑ = 6, 8, 10 for dipole–dipole (d–d), dipole–quadrupole (d–q), quadrupole–quadrupole (q–q) interactions, respectively. Fig. 3b shows the fitting lines of $\log(I/x)$ vs $\log(x)$ in $Ca_9La_{1-x}(PO_4)_5(SiO_4)F_2$:$xDy^{3+}$ phosphors with the different wavelength (485 nm and 580 nm) beyond the quenching concentration. It is clear that the fitting curves of $\lg(I/x)$ vs $\lg(x)$ can be well matched as a relatively linear dependence and the slopes were determined to be -1.97, and -2.08, which corresponds to the $^4F_{9/2}\rightarrow{}^6H_{15/2}$ and $^4F_{9/2}\rightarrow{}^6H_{13/2}$ transition of doped Dy^{3+} ions. Herein, the values of ϑ can be calculated as 5.91 and 6.24, respectively. Both of the obtained ϑ values are close to 6, demonstrating that the interaction type in $Ca_9La(PO_4)_5(SiO_4)F_2$:Dy^{3+} is dipole-dipole interactions.

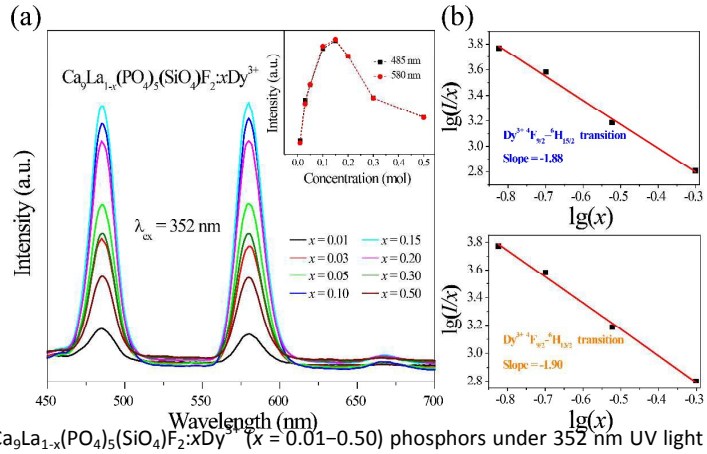

Fig. 3 (a) Emission spectra of $Ca_9La_{1-x}(PO_4)_5(SiO_4)F_2$:$xDy^{3+}$ (x = 0.01–0.50) phosphors under 352 nm UV light excitation. The inset shows the dependence of the emission intensity on the concentration of Dy^{3+}. (b) The fitting curves of $\lg(I/x)$ vs. $\lg(x)$ in $Ca_9La_{1-x}(PO_4)_5(SiO_4)F_2$:$xDy^{3+}$ phosphors.

The PL decay curves and lifetimes of Dy^{3+} for $Ca_9La_{1-x}(PO_4)_5(SiO_4)F_2$:$xDy^{3+}$ (x = 0.01–0.50) phosphors under the excitation of 352 nm by monitoring different emission bands corresponding to the wavelength at 485 and 580 nm are shown in Fig. 4. It is found that all of the decay curves could be fitted successfully with a typical second-order exponential decay equation as follows:

$$I(t) = I_0 + A_1\exp(-t/\tau_1) + A_2\exp(-t/\tau_2) \qquad (4)$$

where I(t) is the luminescence intensity at time t, A_1 and A_2 are constants, t is the time, and τ_1 and τ_2 are rapid and slow times for the exponential components. Herein, the decay processes of these samples are characterized by average lifetime (τ*), which was defined as following formula:

$$\tau^* = (A_1\tau_{12} + A_2\tau_{22})/(A_1\tau_1 + A_2\tau_2) \qquad (5)$$

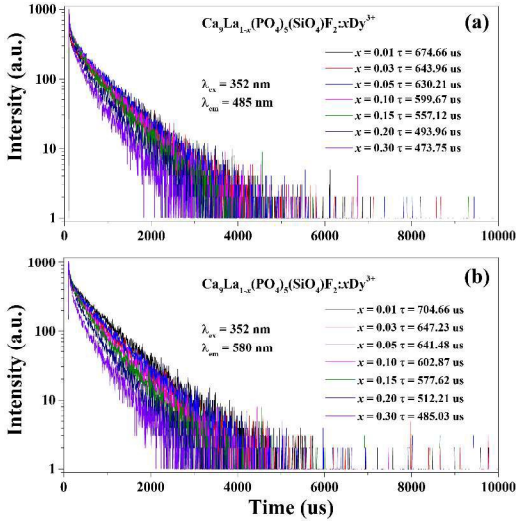

Fig. 4 Decay curves of Dy^{3+} emission in $Ca_9La_{1-x}(PO_4)_5(SiO_4)F_2$:$xDy^{3+}$ (x = 0.01–0.50) phosphors under excitation at 352 nm, monitored at (a) 485 nm and (b) 580 nm.

An obvious phenomenon is found that the decay time begins to decrease gradually with the increasing of Dy^{3+} concentration. The decay lifetimes at 485 nm are estimated to be 674.66 us, 643.96 us, 630.21 us, 599.67 us, 557.12 us, 493.96 us, and 473.75 us. Meanwhile, the decay lifetimes at 580 nm are estimated to be 704.66 us, 647.23 us, 641.48 us, 602.87 us, 577.62 us, 512.21 us, and 485.93 us. The restrained lifetime is related to the total relaxation rate, which can be expressed by: [30]

$$\frac{1}{\tau} = \frac{1}{\tau_0} + A_{\mathrm{nr}} + P_t \qquad (6)$$

Here τ_0 is the radiative lifetime, A_{nr} is the nonradiative rate due to multiphonon relaxation, and P_t is the energy transfer rate between activator Dy^{3+} ions. Considering the distance between Dy^{3+}-Dy^{3+} ions decreases in pace with increasing Dy^{3+} doped concentrations, the probability of energy transfer to luminescent killer sites increased. As a consequence, the lifetimes will be shorten because of supporting the nonradiative energy transfer processes as increasing Dy^{3+} concentration, which is similar to some previous results discussed in other system [30-32].

Table 4. CIE chromaticity coordinates (*x*, *y*) and CCT for $Ca_9La_{1-x}(PO_4)_5(SiO_4)F_2$:*y*$Dy^{3+}$ (*y* = 0.01–0.50) samples (λ_{ex} = 352 nm).

Sample NO.	Sample composition (*y*)	CIE coordinates (*x*, *y*)	CCT (K)
1	y = 0.01	(0.311, 0.313)	6776
2	y = 0.03	(0.338, 0.336)	5262
3	y = 0.05	(0.351, 0.360)	4835
4	y = 0.10	(0.358, 0.366)	4597
5	y = 0.15	(0.356, 0.366)	4663
6	y = 0.20	(0.355, 0.363)	4688
7	y = 0.30	(0.341, 0.349)	5145
8	y = 0.50	(0.335, 0.342)	5401

The variation of chromaticity coordination (*x*, *y*) of $Ca_9La_{1-x}(PO_4)_5(SiO_4)F_2$:*x*$Dy^{3+}$ (*x* = 0.01–0.50) excited under 352 nm are calculated based on the corresponding PL spectrum in the CIE 1931 chromaticity, and the chromaticity coordinates and CCT are summarized in Fig. 5 and Table 4, respectively. It can be seen that the emission colors of all of the as-prepared samples locate in the white light region. As we known, the standard white chromaticity coordination was selected with *x* = 0.333 and *y* = 0.333 in the CIE 1931 chromaticity. Generally, it exhibits a better white emitting quality when the chromaticity coordination closes to the ideal white chromaticity coordination (*x* = 0.333, *y* = 0.333) [33]. Therefore, the optimal chromaticity coordinates and CCT are designed as (*x* = 0.338, *y* = 0.336) and 5262 K, which indicates that $Ca_9La(PO_4)_5(SiO_4)F_2$:Dy^{3+} could serve as a potential single phase white-emitting phosphor in solid-state lighting for white-light *n*-UV LED devices.

The thermal stability of phosphor is one of the important issues for potential applications in high-power LEDs. Fig. 6 shows the temperature-dependent emission spectra for the selected $Ca_9La_{0.85}(PO_4)_5(SiO_4)F_2$:0.15$Dy^{3+}$ phosphor under 390 nm excitation, and the relative emission intensities as a function of temperature were given in the inset of Fig. 6. It can be seen that the PL intensity slowly decreases with increasing temperature. Generally, the phosphors of white LED are require to sustain their emission efficiency up to 150 °C over a long term because the temperature of a LED package rises by the heat generation of LED itself during LED operation. When the temperature rose from room temperature to 150 oC, the PL intensities of $Ca_9La_{0.85}(PO_4)_5(SiO_4)F_2$:0.15$Dy^{3+}$ phosphor decreased to 71% of the initial PL intensity, which indicates that the as-prepared phosphors has great potential application to meet the application requirements for n-UV LEDs.

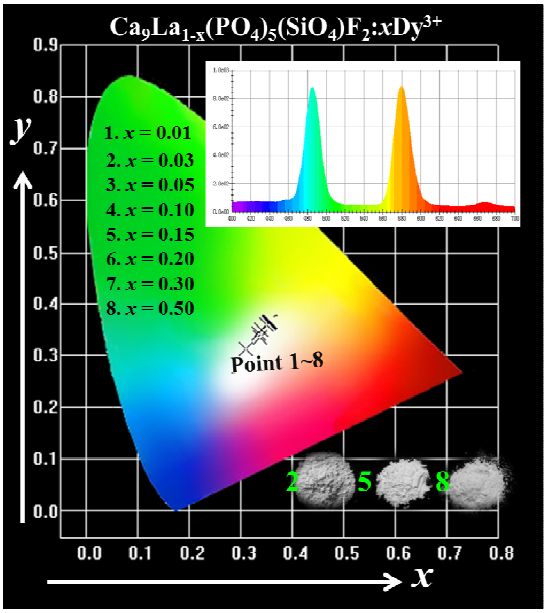

Fig. 5 CIE chromaticity diagram of the selected $Ca_9La_{1-x}(PO_4)_5(SiO_4)F_2$:*x*$Dy^{3+}$ (*x* = 0.01–0.50) phosphors (λ_{ex} = 352 nm), and a digital photograph of white-light emission is also shown as evidence. (Insert) The PL spectrum of $Ca_9La_{0.85}(PO_4)_5(SiO_4)F_2$:0.15$Dy^{3+}$.

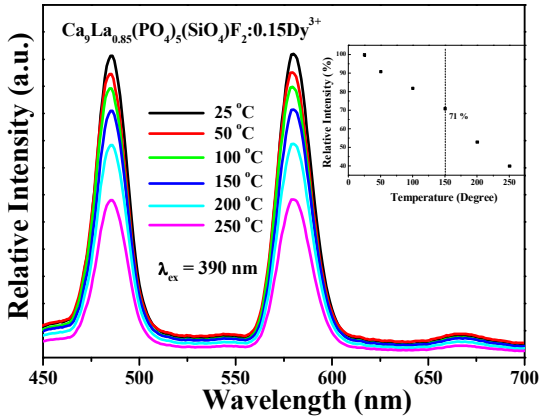

Fig. 6 Temperature-dependent PL spectra of $Ca_9La_{0.85}(PO_4)_5(SiO_4)F_2$:0.15$Dy^{3+}$ under different temperatures in the range of 25-300 ^oC.

4 Conclusions

In summary, a series of novel white-light-emitting phosphors $Ca_9La_{1-x}(PO_4)_5(SiO_4)F_2$:$x$$Dy^{3+}$ were synthesized via a conventional solid-state reaction. Upon 352 nm excitation, these phosphors exhibits two intense emission bands centered at 485 and 580 nm, which ascribes to $^4F_{9/2}\rightarrow{}^6H_{15/2}$ and $^4F_{9/2}\rightarrow{}^6H_{13/2}$ transitions of Dy^{3+} , respectively. The spectroscopic data and fluorescence decay dynamics indicate that the energy transfer process takes place between Dy^{3+}-Dy^{3+} ions via a nonradiative dipole-dipole mechanism. All of the chromaticity coordinates of $Ca_9La_{1-x}(PO_4)_5(SiO_4)F_2$:$x$$Dy^{3+}$ are located in the proximity of the standard white chromaticity coordination, demonstrating $Ca_9La(PO_4)_5(SiO_4)F_2$:Dy^{3+} can be regarded as a potential candidate in solid-state lighting combing with blue chip or near-UV chip.

Acknowledgements

We gratefully acknowledge the financial support by the National Natural Science Foundations of China (Grant nos. 41172053), the Fundamental Research Funds for the Central Universities (Grant no. 2652013043), and Science and Technology Innovation Fund of the China University of Geosciences (Beijing).

Notes and references

1 M.M. Shang, C.X. Li and J. Lin, *Chem. Soc. Rev.*, 2014, **43**, 1372.
2 W. Lv, Z. D. Hao, X. Zhang, Y. S. Luo, X. J. Wang and J. H. Zhang, *Inorg. Chem.*, 2011, **50**, 7846.
3 S. Tonzani, *Nature*., 2009, **459**, 312.
4 C. H. Huang and T. M. Chen, *J. Phys. Chem. C.*, 2011, **115**, 2349.
5 H.K. Liu, Y.Y. Zhang, L.B. Liao and Z.G. Xia, *J. Lumin.*, 2014, **156**, 49.
6 F.W. Kang, Y. Zhang and M.Y. Peng, *Inorg. Chem.*, 2015, **54**, 1462.
7 G. Zhu, Y.H. Wang, Z.P. Ci, B.T. Liu, Y.R. Shi and S.Y. Xin, *J. Electrochem. Soc.*, 2011, **158,** J236.
8 M.M. Shang, G.G. Li, D.L. Geng, D.M. Yang, X.J. Kang, Y. Zhang, H.Z. Lian and J. Lin, *J. Phys. Chem. C.*, 2012, **116**, 10222.
9 D. Mazza, M. Tribaudino, A. Delmastro and B. Lebech, *J. Solid State Chem.*, 2000, **155**, 389.
10 M.M. Jiao, N. Guo, W. Lv, Y.C. Jia, W.Z. Lv, Q. Zhao, B.Q. Shao and H.P. You, *Inorg. Chem.*, 2013, **52**, 10340.
11 H. B. Liang, Q. Zeng, and Z. F. Tian, *J. Electrochem. Soc.*, 2007, **154**, J177.
12 X. Chen, P. Dai, X.Zhang, C. Li, S. Lu, X. Wang, Y. Jia and Y. Liu, *Inorg. Chem.*, 2014, **53**, 3441.
13 Y.I. Jeon, K. Bharat and J.S. Yu, *J. Alloy. Compd.*, 2015, **620**, 263.
14 J. Lin and Q. Su, *J. Mater. Chem.*, 1995, **5**, 1151.
15 H.K. Liu, Y. Luo, Z.Y. Mao, L.B. Liao and Z.G. Xia, *J. Mater. Chem. C.*, 2014, **2**, 1619.
16 Q. Long, C. Wang, Y.Y. Li, J.Y. Ding, X.C. Wang and Y.H. Wang, *Mater. Res. Bull.*, 2015, **71**, 21.
17 M.H. Tong, Y.J. Liang, G.G. Li, Z.G. Xia, M.F. Zhang, F. Yang and Q. Wang, *Opt. Mater.*, 2014, **36**, 1566.
18 Z.P. Ci, Q.S. Sun, S.C. Qin, M.X. Sun, X.J. Jiang, X.D. Zhang and Y.H. Wang, *Phys. Chem. Chem. Phys.*, 2014, **16**, 11597.
19 Z.W. Zhang, A.J. Song, Y. Yue, H. Zhong, X.Y. Zhang, M.Z. Ma and R.P. Liu, *J. Alloy. Compd.*, 2015, **650**, 410.
20 Bruker AXS TOPAS V4: General profile and structure analysis software for powder diffraction data. User's Manual. Bruker AXS, Karlsruhe, Germany. 2008.
21 H. Njema, K. Boughzala, H. Boughzala and K. Bouzouita, *J. Rare. Earth.*, 2013, **31**, 897.
22 H. Njema, M. Debbichi, K. Boughzala, M. Said and K. Bouzouita, *Mater. Res. Bull.*, 2014, **51**, 210.
23 R. D. Shannon, Acta Crystallogr., *Sect. A: Cryst. Phys., Diffr., Theor. Gen. Crystallogr.*, 1976, **32**, 751.
24 G. Blasse and B. C. Grabmaier, Luminescent Materials., Springer Verlag, Berlin, 1994.
25 H. Yu, D.G. Deng, D.T. Zhou, W. Yuan, Q.E. Zhao, Y.J. Hua, S.L. Zhao, L.H. Huang, S.Q. Xu, *J. Mater. Chem. C.*, 2013, **1**, 5577.
26 H.K. Liu, Y.Y. Zhang, L.B. Liao, Q.F. Guo and L.F. Mei, *Ceram. Inter.*, 2014, **40**, 13709.
27 G. G. Li, D. L. Geng, M. M. Shang, C. Peng, Z. Y. Cheng and J. Lin, *J. Mater. Chem.*, 2011, **21**, 13334.
28 G. Blasse, W. L. Wanmaker, J. W. Tervrugt, and A. Bril, *Philips. Res. Rep.*, 1968, **23**, 189.
29 H. Jing, C.F. Guo, G.G. Zhang, X.Y. Su, Z. Yang and J.H. Jeong, *J. Mater. Chem.*, 2012, **22**, 13612.
30 Z.G. Xia, H.K. Liu, X. Li and C.Y. Liu, Dalton. Trans., 2013, **42**, 16588.
31 G. Y. Lee, J. Y. Han, W. B. Im, S. H. Cheong and D. Y. Jeon, *Inorg. Chem.*, 2012, **51**, 10688.
32 J. Y. Han, W. B. Im, G. Y. Lee and D. Y. Jeon, *J. Mater. Chem.*, 2012, **22**, 8793.
33 Z. Y. Mao, Y. C. Zhu, Y. Wang, and L. Gan, *J. Mater. Sci.*, 2014, **49**, 4439.

A novel single-phase white light emitting phosphor $Ca_9La(PO_4)_5(SiO_4)F_2:Dy^{3+}$: synthesis, crystal structure and luminescence property

Haikun Liu[a], Libing Liao[a,*], Maxim S. Molokeev[b,c], Qingfeng Guo[a], Yuanyuan Zhang[a], Lefu Mei[a,*]

[a]*Beijing Key Laboratory of Materials Utilization of Nonmetallic Minerals and Solid Wastes, National Laboratory of Mineral Materials, School of Materials Science and Technology, China University of Geosciences, Beijing100083, China*

[b]*Laboratory of Crystal Physics, Institute of Physics, SB RAS, Krasnoyarsk 660036, Russia*

[c]*Department of Physics, Far Eastern State Transport University, Khabarovsk 680021, Russia*